

Thermalization in a Quasi-one-dimensional Quantum Gas

Shovan Dutta*

Laboratory of Atomic and Solid State Physics, Cornell University, Ithaca, New York 14850, USA

(Dated: July 20, 2015)

We model thermalization in a quantum gas loaded into an array of weakly-coupled parallel one-dimensional tubes produced by turning on a lattice in the transverse plane. We derive rate equations for the momentum distribution along the tubes by analyzing binary elastic collisions. For small inter-tube coupling J , the rate of thermalization grows as $J^2 \ln J$. We show that the equilibration times in two recent experiments [Nature **467**, 567 (2010)] and [Nature **440**, 900 (2006)] differ hugely from one another, which provides justification for their apparently conflicting observations. We highlight the qualitative differences in the approach to equilibrium after an adiabatic and a sudden turn-on of the lattice. In particular, we find that for a sudden turn-on, the momentum distribution develops isolated peaks at short times, which can be probed in future experiments.

Introduction.—The remarkable progress in trapping and cooling atoms in recent years has enabled the experimental study of many-body quantum systems in different dimensions [1]. In particular, using a suitable laser configuration it is now possible to trap atoms in highly elongated tubes, effectively confining their motion to one dimension (1D) [2–7]. Reducing the dimensionality of a system enhances correlation effects among the particles, and can lead to exotic quantum phases not present in higher dimensions. A prime example of such a phase is the modulated superconducting phase (also known as FFLO) in a population-imbalanced two-component Fermi gas with attractive interactions [5, 8–14]. When the two spin components (\uparrow, \downarrow) have equal populations, an \uparrow -spin forms a Cooper pair with a \downarrow -spin, leading to Bardeen-Cooper-Schrieffer (BCS) superconductivity with a uniform order parameter. However, when they have unequal populations, their Fermi surfaces mismatch, which destabilizes the BCS phase. It was predicted from theory that the ground state of such a system in 1D is a partially spin-polarized superconducting phase with an order parameter which oscillates in space. Such a partially polarized phase was indeed observed in a recent experiment at Rice with ${}^6\text{Li}$ atoms [5]. The experimental data fit very well with the phase diagram calculated from the thermodynamic Bethe ansatz. However, the theoretical model assumes that the system is in thermal equilibrium. But it is well known that an isolated 1D system cannot thermalize due to kinematic constraints [6, 15–19]. In higher dimensions, thermalization occurs via elastic collisions among the particles, which redistribute their momenta, thus allowing the system to ergodically sample all momentum states. However, in 1D, conservation of both momentum and energy implies that particles can only exchange momenta in a collision. Therefore no new momentum states are occupied, and the system fails to thermalize. This fact was confirmed in another recent experiment [6] where Kinoshita *et al.* prepared bosonic ${}^{87}\text{Rb}$ atoms in a highly elongated trap in an out-of-equilibrium state. The system did not thermal-

ize even after thousands of collisions. The resolution to the apparent conflict between the two experiments rests in the fact that real set-ups are not perfectly 1D. The particles still have some leftover degrees of freedom to move in the other two dimensions, which allows the system to thermalize at long times. Here we model thermalization in such quasi-1D systems using quantum kinetic rate equations.

In a typical experiment such as [5], the experimentalists first prepare atoms of mass m in a three-dimensional (3D) harmonic trap. Then they turn on a deep lattice potential in the x - y plane. As a result, the atoms are captured in an array of elongated tubes along the z direction. In a deep lattice, the potential near a lattice site is well-approximated by a harmonic well of frequency ω . This transverse confinement frequency is typically 2-3 orders of magnitude larger than the axial trapping frequency. Thus the particles are essentially free to move along the tubes in the z -direction. The state of the atoms after the lattice is turned on depends on how fast the lattice is turned on compared to the collision rate among particles. In both [5] and [6], the lattice turn-on time is large compared to the collision time, allowing the system to relax to the lowest band. Since the atom energies are much smaller than the band gap $\hbar\omega$, the subsequent dynamics are confined to the lowest band. We first discuss thermalization under such conditions. One can also imagine experiments where the lattice is turned on suddenly. Then the atoms will also populate higher bands. We model this situation in the latter part of the paper, and find that it gives rise to qualitatively different dynamics en route to equilibrium.

Particles in the lowest band.—When the particles are confined to the lowest band, the single-particle Hamiltonian reduces to the tight-binding model, characterized by a tunneling amplitude J . J describes particle hopping between adjacent tubes. The dynamics depend on the dimensionless ratio $\tilde{J} \equiv \pi^2(J/E_R)$, where E_R is the lattice recoil energy. J/E_R decreases with the depth of the lattice. For an infinitely deep lattice, $\tilde{J} = 0$, so the motion is strictly 1D, and no thermalization occurs. Here we study the case where \tilde{J} is small but non-zero, which allows the system to equilibrate. In our model,

* sd632@cornell.edu

equilibration occurs through redistribution of momenta resulting from two-body elastic collisions. In an ultracold experimental setting, collisions are predominantly s -wave, parametrized by a scattering length a_s that can be tuned via a Feshbach resonance [20]. We find that, in units of $m\omega^2 a_s^2$, the thermalization rate grows with \tilde{J} as $J^2(a - b \ln \tilde{J})$, where a and b are set by the initial occupations of the momentum states. For the experimental conditions in [6], our numerics suggest a thermalization time ~ 20 min, which is large compared to the duration of the experiment, which is ~ 0.4 s. This justifies the observed lack of thermalization. In the other experiment [5], the tunneling parameter \tilde{J} is much larger. We estimate an upper bound for the thermalization time of a few μ s, which is 3 orders of magnitude smaller than the observation timescale. This explains why the experimental data agrees so well with thermodynamic calculations. Our analysis is based on the quantum Boltzmann equation for the occupations of the momentum states. For simplicity, here we do not model mean-field interaction effects which modify the energy of the single-particle states [21]. Therefore our model is valid when the physics is not dominated by interactions. Below we outline our analysis in further detail.

We consider a two-component Fermi gas (labeled by spin $\sigma = \uparrow, \downarrow$) loaded into a two-dimensional (2D) optical lattice potential $V_{\text{lat}}(x, y) = V_0(\sin^2(\pi x/a) + \sin^2(\pi y/a))$. We consider a deep lattice with $V_0 \gg E_R$ where E_R is the recoil energy, $E_R = \pi^2 \hbar^2 / (2ma^2)$. The system is described by the Hamiltonian

$$H = H_0 + H_{\text{int}}, \quad (1)$$

where the kinetic and interaction parts are given by

$$H_0 = \int d^3r \sum_{\sigma} \psi_{\sigma}^{\dagger}(\vec{r}) \left(-\frac{\hbar^2}{2m} \nabla^2 + V_{\text{lat}}(x, y) \right) \psi_{\sigma}(\vec{r}) \quad (2)$$

$$H_{\text{int}} = \frac{4\pi \hbar^2 a_s}{m} \int d^3r \psi_{\uparrow}^{\dagger}(\vec{r}) \psi_{\downarrow}^{\dagger}(\vec{r}) \psi_{\downarrow}(\vec{r}) \psi_{\uparrow}(\vec{r}). \quad (3)$$

Here $\psi_{\sigma}(\vec{r})$ denotes the fermion field operator, and H_{int} describes interactions among the particles by a short-range pseudopotential characterized by the s -wave scattering length a_s . We will treat H_{int} as a perturbation which induces transitions among the single-particle eigenstates via two-body elastic collisions.

When the dynamics are confined to the lowest band, we can label the single-particle eigenstates by quasimomenta k_x and k_y in the x - y plane, and momentum k_z along the z direction :

$$\psi_{k_x, k_y, k_z}(\vec{r}) = \frac{1}{\sqrt{L}} e^{ik_z z} \phi_{k_x}(x) \phi_{k_y}(y) \quad (4)$$

$$= \frac{1}{N\sqrt{L}} e^{ik_z z} \sum_{j_x, j_y} e^{i(k_x j_x + k_y j_y)} w_{j_x}(x) w_{j_y}(y) \quad (5)$$

Here L denotes the length over which the particles can move along the z direction. We will consider the limit $L \rightarrow \infty$. ϕ_k denotes the Bloch state with momentum k , which we have expanded in terms of the N Wannier states w_j localized at the N lattice sites j . For deep lattices, the Wannier state $w_j(x)$ is a Gaussian centered at site j : $w_j(x) = \pi^{-1/4} d^{-1/2} \exp(-(x - ja)^2 / (2d^2))$, where $d = \sqrt{\hbar / (m\omega)}$, ω being the transverse confinement frequency, $\omega = (2E_R / \hbar) \sqrt{V_0 / E_R}$. The single-particle state in Eq. (4) has energy

$$\varepsilon(k_x, k_y, k_z) = -2J(\cos k_x + \cos k_y) + \hbar^2 k_z^2 / (2m), \quad (6)$$

where J is the tunneling amplitude in the tight-binding model corresponding to the Hamiltonian H_0 . J decreases exponentially with V_0 / E_R for large lattice depths : $J \approx (4E_R / \sqrt{\pi})(V_0 / E_R)^{3/4} \exp(-2\sqrt{V_0 / E_R})$ [22].

We consider the growth of the \uparrow -spin population $n^{\uparrow}(\vec{k})$ in state $\psi_{\vec{k}}$, where \vec{k} denotes (k_x, k_y, k_z) . This occurs by means of elastic collisions between an \uparrow -spin and a \downarrow -spin, which scatter the \uparrow -spin into the state $\psi_{\vec{k}}$. In such a process, the total energy and z -momentum are conserved, and quasimomenta along x and y are conserved up to one reciprocal lattice constant $2\pi/a$. The rate of such a process is proportional to the populations of the initial states $n^{\uparrow}(\vec{k}_1)$ and $n^{\downarrow}(\vec{k}_2)$. In addition, the exclusion principle for fermions prohibits the process if the final states $\psi_{\vec{k}}$ and $\psi_{\vec{k}_3}$ are already occupied by an \uparrow -spin and a \downarrow -spin respectively. This gives rise to the Pauli blocking factors $1 - n^{\uparrow}(\vec{k})$ and $1 - n^{\downarrow}(\vec{k}_3)$. The collision rate is also proportional to the transition probability between the initial and the final states. We calculate this using Fermi's golden rule, which yields the factor $|\langle \psi_{\vec{k}_1} \psi_{\vec{k}_2} | H_{\text{int}} | \psi_{\vec{k}} \psi_{\vec{k}_3} \rangle|^2$. Combining all these terms, we arrive the kinetic rate equation (with $\tilde{k} \equiv ka$)

$$\frac{dn^{\uparrow}(\tilde{k})}{dt} = \frac{16\pi}{\hbar} m\omega^2 a_s^2 \times$$

$$\int_{-\infty}^{\infty} \frac{d\tilde{k}_{z1}}{2\pi} \int_{-\infty}^{\infty} \frac{d\tilde{k}_{z2}}{2\pi} \int_{-\pi}^{\pi} \frac{d\tilde{k}_{x1}}{2\pi} \int_{-\pi}^{\pi} \frac{d\tilde{k}_{y1}}{2\pi} \int_{-\pi}^{\pi} \frac{d\tilde{k}_{x2}}{2\pi} \int_{-\pi}^{\pi} \frac{d\tilde{k}_{y2}}{2\pi}$$

$$\times [n^{\uparrow}(\tilde{k}_1) n^{\downarrow}(\tilde{k}_2) (1 - n^{\uparrow}(\tilde{k})) (1 - n^{\downarrow}(\tilde{k}_1 + \tilde{k}_2 - \tilde{k}))$$

$$- (1 - n^{\uparrow}(\tilde{k}_1)) (1 - n^{\downarrow}(\tilde{k}_2)) n^{\uparrow}(\tilde{k}) n^{\downarrow}(\tilde{k}_1 + \tilde{k}_2 - \tilde{k})]$$

$$\times \delta(\tilde{k}_z^2 + (\tilde{k}_{z1} + \tilde{k}_{z2} - \tilde{k}_z)^2 - \tilde{k}_{z1}^2 - \tilde{k}_{z2}^2 +$$

$$2\tilde{J}(\cos \tilde{k}_{x1} + \cos \tilde{k}_{x2} - \cos \tilde{k}_x - \cos(\tilde{k}_{x1} + \tilde{k}_{x2} - \tilde{k}_x))$$

$$+ \cos \tilde{k}_{y1} + \cos \tilde{k}_{y2} - \cos \tilde{k}_y - \cos(\tilde{k}_{y1} + \tilde{k}_{y2} - \tilde{k}_y)) \quad (7)$$

Hereafter we assume that the energy distribution of the particles has a width much larger than J , so that all quasimomentum states are equally populated, i.e., $n^{\sigma}(k_x, k_y, k_z) \approx n^{\sigma}(k_z)$. This is a valid approximation

in most quasi-1D experiments [5, 6], and significantly reduces the computational cost. Then $\int n^\sigma(k_z)dk_z$ gives the linear density of spin- σ particles along the z -direction at each lattice site. For simplicity, we limit our analysis to the case where the \uparrow - and \downarrow -spins are equally distributed among the momentum states, i.e., $n^\sigma(k_z) = n(k_z)$. We have studied the case of unequal populations, and found that the main features remain unaltered as long as the imbalance is not too large. In addition, making this assumption also allows us to apply our formalism to spinless bosons [6]. As opposed to fermions, bosons have a greater likelihood of scattering into a state k_z which is already occupied. Hence we will have a Bose enhancement factor $(1 + n(k_z))$ in place of the Pauli blocking factor $(1 - n(k_z))$. With these considerations, we can simplify Eq. (7) to obtain (see Appendix A for details)

$$\begin{aligned} \frac{dn(k)}{d\tau} = & \int_{-\infty}^{\infty} dp \int_{-\infty}^{\infty} dq f(pq) \times \\ & \left[n(k + \tilde{J}^{\frac{1}{2}}p)n(k + \tilde{J}^{\frac{1}{2}}q)(1 + \zeta n(k))(1 + \zeta n(k + \tilde{J}^{\frac{1}{2}}(p + q))) \right. \\ & \left. - (1 + \zeta n(k + \tilde{J}^{\frac{1}{2}}p))(1 + \zeta n(k + \tilde{J}^{\frac{1}{2}}q))n(k)n(k + \tilde{J}^{\frac{1}{2}}(p + q)) \right] \end{aligned} \quad (8)$$

where $\tau = 2m\omega^2 a_s^2 / (\pi\hbar)$, $k \equiv \tilde{k}_z$, and $\zeta = +1$ for bosons and -1 for fermions. The function f results from integrating out the delta function in Eq. (7) over the quasi-momenta, and is given by

$$f(\xi) = \frac{1}{2\pi} \int_{-\infty}^{\infty} du e^{i\xi u} \left({}_2F_3\left(\frac{1}{2}, \frac{1}{2}; 1, 1, 1; -4u^2\right) \right)^2. \quad (9)$$

It is peaked about $\xi = 0$ and vanishes for $|\xi| > 8$.

Since we are interested in quasi-1D experiments where \tilde{J} is small, it is useful to expand Eq. (8) in powers of \tilde{J} . However, a direct Taylor expansion proves difficult because although the product Jpq is restricted to small values, either of $\tilde{J}^{1/2}p$ or $\tilde{J}^{1/2}q$ can be very large. Physically, this means that there are two kinds of energy-conserving collisions which populate state k : (i) collisions where both particles have momenta close to k , and (ii) collisions where one particle has momentum very different from k , and the other particle has momentum $\approx k$. The difficulty in obtaining an asymptotic expansion is bypassed if one transforms Eq. (8) into the Fourier domain $\tilde{n}(x)$. We carry out the expansion in the Fourier domain, and then perform an inverse transform to get the following expressions (see Appendix B for details)

$$\dot{n}(k) = (\dot{n}(k))_{\text{cl}} + (\dot{n}(k))_{\text{qu}} + \mathcal{O}(\tilde{J}^4 \ln \tilde{J}), \quad (10)$$

with

$$(\dot{n}(k))_{\text{cl}} = \tilde{J}^2 \left[\left((3 - \ln \tilde{J})I_2 - I_{2l} \right) \mathcal{F}_1[n(k)] + I_2 \mathcal{F}_2[n(k)] \right] \quad (11)$$

$$\begin{aligned} (\dot{n}(k))_{\text{qu}} = & \\ & \zeta \tilde{J}^2 \left[\left((3 - 2\gamma - \ln(\tilde{J}/4))I_2 - I_{2l} \right) \mathcal{F}_3[n(k)] + I_2 \mathcal{F}_4[n(k)] \right]. \end{aligned} \quad (12)$$

Here $\dot{n}(k) \equiv dn(k)/d\tau$, $I_2 = \int_0^\infty d\xi \xi^2 f(\xi) \approx 2$, and $I_{2l} = \int_0^\infty d\xi \xi^2 \ln \xi f(\xi) \approx 2.18$, and γ denotes the Euler's constant. Eq. (10) shows that the net dynamics can be broken up into a classical part $(\dot{n}(k))_{\text{cl}}$ and a quantum part $(\dot{n}(k))_{\text{qu}}$. Here $\zeta = +1$ for bosons, -1 for fermions, and 0 for distinguishable particles. The expressions for the functionals $\mathcal{F}_i[n(k)]$, $i = 1, 2, 3, 4$ in Eqs. (11) and (12) are given in Eqs. (B5)-(B8). We have simulated the dynamics using both the full rate equation in Eq. (8) and the asymptotic expressions in Eqs. (10-12), and found excellent agreement between the two for $\tilde{J} \lesssim 0.01$.

From Eqs. (11) and (12) we see that the thermalization rate, in units of $m\omega^2 a_s^2 / \hbar$, grows with \tilde{J} as $\tilde{J}^2(a - b \ln \tilde{J})$ where the coefficients a and b are set by $n(k)$. In Fig. 1 we show how $n(k)$ evolves with time for $\tilde{J} = 0.001$, after starting from a double-peaked non-equilibrium profile, $n(k, t=0) = (1/2)(\exp(-8(k+1)^2) + \exp(-8k^2) + \exp(-8(k-1)^2))$, corresponding to a linear density of $\approx 0.47/a$. We plot $n(k, t)$ for bosons and fermions. We see that bosons thermalize faster than fermions. This is expected since bosons experience Bose enhancement which assists two-body collisions, whereas fermions experience Pauli blocking which reduces the collision rate. However, for state occupations $\lesssim 0.5$, we find that both classes of particles exhibit similar dynamics. To quantify the approach toward a thermal state, we calculate $\delta = \int (n(k) - n_{\text{th}}(k))^2 / (\int n(k)dk)^2$, where $n_{\text{th}}(k)$ denotes

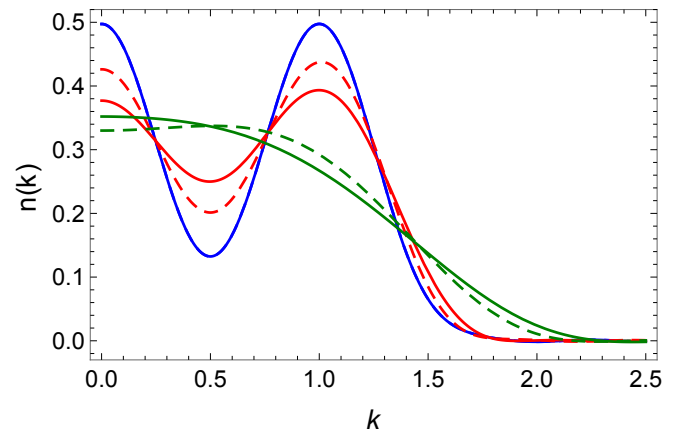


FIG. 1. Time evolution of the momentum distribution $n(k)$ for $\tilde{J} = 0.001$. The blue, red, and green curves correspond to $t/t_0 = 0, 200$, and 4500 respectively. Solid lines stand for bosons, and dashed lines stand for fermions.

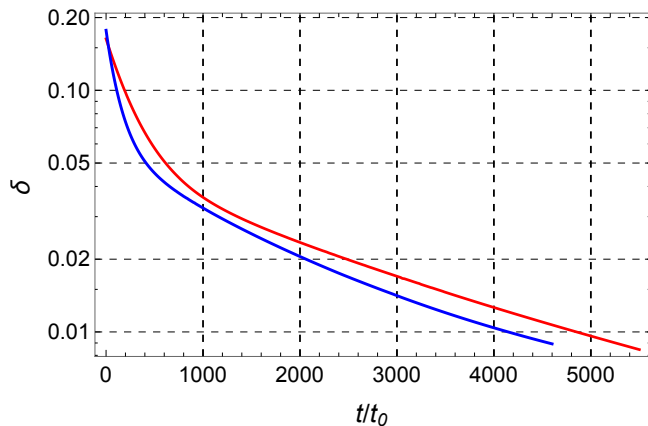


FIG. 2. Mismatch δ (defined in the text) between $n(k)$ and its thermal fit, plotted as a function of time. The blue curve stands for bosons, and the red curve stands for fermions.

the thermal fit to $n(k)$. δ describes the mismatch between $n(k)$ and a thermal distribution. In Fig. 2, we plot δ as a function of time for the same initial conditions as in Fig. 1. We see that the particle distribution monotonically approaches a thermal state at long times. Taking a cut-off of 0.01 for δ we obtain a thermalization time $t_{\text{th}} \sim 5 \times 10^3 t_0$, where $t_0 = \pi\hbar/(2m\omega^2 a_s^2)$.

We now estimate the thermalization times for the experimental set-ups in Refs. [5] and [6]. In Ref. [6], Kinoshita *et al.* prepare a gas of ^{87}Rb atoms having scattering length $a_s = 5.3$ nm in highly elongated tubes with a transverse confinement frequency $\omega = 2\pi \times 67$ kHz. This gives $t_0 \approx 0.23$ ms. They use a deep lattice in the x - y plane with a lattice spacing $a = 386.5$ nm. Using ω and a we can calculate $V_0/E_R = (\hbar\omega/(2E_R))^2 \approx 76$, and therefore the tunneling amplitude $\tilde{J} \approx 4\pi^{3/2}(V_0/E_R)^{3/4} \exp(-2\sqrt{V_0/E_R}) = 1.5 \times 10^{-5}$. The linear density of ^{87}Rb atoms in the experiment is $\sim 5 \times 10^6 \text{m}^{-1} \approx 1.93/a$. Comparing these values with those used in plotting Figs. 1 and 2, we find that although the linear density is about 4 times larger in the experiment, the tunneling amplitude \tilde{J} is about 66 times smaller. Since we have seen that for small \tilde{J} , the thermalization rate grows as $\tilde{J}^2 \ln \tilde{J}$ (Eqs. (10)-(12)), and we expect the rate to grow linearly with the particle density, we conclude that the thermalization time t_{th} for the experimental system in [6] would be much larger than $5 \times 10^3 t_0 = 1.15$ s. As a rough estimate, we get $t_{\text{th}} \sim (1/4)(66^2)(1.15 \text{ s}) \sim 20$ min. This justifies why no signature of thermalization was observed within the experimental duration of ~ 0.4 s.

On the other hand, in Ref. [5], Liao *et al.* load ^6Li atoms into a 2D array of elongated tubes with a transverse confinement frequency $\omega = 4\pi \times 10^5$ Hz. They perform their experiment close to a Feshbach resonance. Hence the ^6Li atoms have a large scattering length, $a_s \approx -484$ nm. Using these parameters, we get $t_0 \approx 45$ ns. The lattice spacing in the x - y plane is $a = 532$

nm. This yields $V_0/E_R \approx 11.6$, and $\tilde{J} \approx 0.15$. The linear density of particles along the tubes near $z = 0$ is $\sim 10^7 \text{cm}^{-1} \approx 5/a$. We see that both the linear density and the tunneling amplitude are much larger than those used in Figs. 1 and 2. Therefore, the thermalization time t_{th} would be much smaller than $5 \times 10^3 t_0 = 0.22$ ms. Since the experiment occurs in the strongly interacting regime, one would need to modify our kinetic equations to get an accurate measure for t_{th} . However, based on the orders of magnitude involved, we can safely say that the system would equilibrate within a few μs , which is about a thousand times smaller than the timescale of observations. This explains why the experimental measurements agree with thermodynamic calculations.

In summary, a non-zero tunneling amplitude \tilde{J} allows the particles to hop between adjacent tubes. This motional degree of freedom in the x - y plane allows the redistribution of the z -momenta via two-body elastic collisions, eventually leading to thermalization. In the limit of small \tilde{J} , we get a diffusion-like equation (Eqs. (8)-(12)) for the momentum occupations $n(k)$. The initial non-equilibrium profile “spreads out” gradually, and monotonically approaches a thermal distribution, as in Figs. (10)-(12)). The thermalization rate is proportional to $m\omega^2 a_s^2$, and increases with \tilde{J} and the particle density. It vanishes at $\tilde{J} = 0$, and grows as $\tilde{J}^2(a - b \ln \tilde{J}) + \mathcal{O}(\tilde{J}^4)$ for small \tilde{J} , where a and b are set by $n(k)$.

Particles in discrete energy levels.—Up to now, we have considered the situation where the particles are free to move along each tube in the z direction, but their x - y motion is confined to the lowest band of the lattice. Such a scenario arises in experiments where the lattice in the x - y plane is turned on adiabatically, i.e. slowly compared to the collision rate among the particles. This is true in both experiments [5] and [6]. However, one can imagine an experiment where the particles are first collected in a 3D harmonic trap, then a lattice potential is turned on suddenly in the x - y plane. Here the particles would not get time to relax to the lowest band during the lattice turn on. In the following we model the subsequent dynamics toward thermalization under such conditions.

We consider the situation where the lattice depth is large, $V_0/E_R \gg 1$, so that the low-lying energy bands reduce to a series of equispaced energy levels. This amounts to assuming zero tunneling between adjacent tubes, and replacing the lattice potential at each tube by a harmonic confinement of frequency ω . The atoms will then populate several of these harmonic oscillator states after the lattice is turned on. The reason for making the harmonic approximation is two-fold: first, it simplifies the analysis and keeps the problem computationally tractable. Second, it allows us to study the qualitative differences in the approach to equilibrium between the two cases, one where the x - y degrees of freedom originate from a set of discrete energy levels, and the other where they originate from a continuum of states within a band.

Here we label the single-particle states by n_x , n_y , and k_z , where (n_x, n_y) denotes the eigenstates of

the 2D harmonic oscillator, and k_z labels the z -momentum. The wavefunction ϕ and energy ε corresponding to this state are given by $\phi_{n_x, n_y, k_z}(\vec{r}) = (1/(L^{1/2}d))\chi_{n_x}(x/d)\chi_{n_y}(y/d)\exp(ik_z z)$, and $\varepsilon_{n_x, n_y, k_z} = (n_x + n_y + 1)\hbar\omega + \hbar^2 k_z^2/(2m)$, where d is the harmonic oscillator length, $d = (\hbar/(m\omega))^{1/2}$, and $\chi_n(x) = \exp(-x^2/2)H_n(x)/\sqrt{2^n n! \sqrt{\pi}}$, H_n being the Hermite polynomial of degree n .

By analyzing the rate of two-body elastic collisions in the same way as presented earlier, we arrive at the rate equation governing the growth of particle population in the state (n_x, n_y, k_z) :

$$\begin{aligned} \frac{dn_{\vec{n}}(k)}{d\tau} = & \sum_{\vec{n}_1, \vec{n}_2, \vec{n}_3} \mathcal{C}(n_x, n_{x_1}, n_{x_2}, n_{x_3}) \mathcal{C}(n_y, n_{y_1}, n_{y_2}, n_{y_3}) \\ & \int' \frac{dp}{q} \left[n_{\vec{n}_1}(p+q)n_{\vec{n}_2}(p-q)(1+\zeta n_{\vec{n}}(k))(1+\zeta n_{\vec{n}_3}(2p-k)) \right. \\ & \left. - (1+\zeta n_{\vec{n}_1}(p+q))(1+\zeta n_{\vec{n}_2}(p-q))n_{\vec{n}}(k)n_{\vec{n}_3}(2p-k) \right], \end{aligned} \quad (13)$$

where $\vec{n} \equiv (n_x, n_y)$, $k \equiv k_z d$, $\tau = (4m\omega^2 a_s^2/(\pi^3 \hbar))t$,

$$q = \sqrt{(p-k)^2 + n_x + n_{x_3} - n_{x_1} - n_{x_2} + n_y + n_{y_3} - n_{y_1} - n_{y_2}}, \quad (14)$$

and the prime over the integration symbol restricts the integrand to regions where q is real. The coefficient \mathcal{C} is defined as the overlap $\mathcal{C}(n, n_1, n_2, n_3) = 2\pi^2 \left| \int_{-\infty}^{\infty} dx \chi_n(x)\chi_{n_1}(x)\chi_{n_2}(x)\chi_{n_3}(x) \right|^2$ which vanishes if $n + n_1 + n_2 + n_3$ is odd, and otherwise has the expression

$$\begin{aligned} & \frac{1}{n!n_1!n_2!n_3!} \left(\frac{\Gamma(\frac{n+n_3+n_1-n_2+1}{2})\Gamma(\frac{n-n_3+n_1+n_2+1}{2})}{\Gamma(\frac{n-n_3+n_1-n_2+1}{2})} \right)^2 \times \\ & \left({}_3F_2 \left(\begin{matrix} -n, & -n_1, & \frac{-n+n_3-n_1+n_2+1}{2} \\ \frac{-n-n_3-n_1+n_2+1}{2}, & \frac{-n+n_3-n_1-n_2+1}{2} \end{matrix}; 1 \right) \right)^2. \end{aligned} \quad (15)$$

As before, $\zeta = +1$ for bosons, -1 for fermions, and 0 for distinguishable particles in Eq. (13). In the following we limit our consideration to fermions for simplicity. The qualitative features remain the same for bosons unless the occupation numbers are large.

We simulate the dynamics using Eq. (13) taking non-equilibrium initial states where the k distribution is narrow compared $1/d$. This is because in experiments, prior to the lattice turn on, the trapped atoms are at a temperature T which is small compared to the band gap $\hbar\omega$. We find three different timescales in the dynamics. The different states within a given energy level $n_x + n_y = M$ attain equal population within a few collision times. It takes longer for the total populations in different energy levels to reach a thermal distribution. The slowest timescale in the dynamics is the equilibration of the momentum states k , which takes several hundred collision times. We compute the collision time τ_{coll} by first fitting

the initial distribution to a thermal one, then using the thermal fit to calculate $\tau_{\text{coll}} = 1/(4\pi a_s^2 n v)$, where n and v denote the average 3D density and the average speed of the particles.

Since the states within a given energy level quickly reach equal population, we simplify the full dynamics in Eq. (13) by assuming that they are always equally populated, i.e., $n_{\vec{n}}(k) = n_M(k)$, where $n_x + n_y = M$. Thus we obtain the following rate equation for $n_M(k)$

$$\begin{aligned} \frac{dn_M(k)}{d\tau} = & \frac{1}{M+1} \sum_{M_1, M_2, M_3=0}^{\infty} F(M, M_1, M_2, M_3) \int' \frac{dp}{q} \times \\ & \left[n_{M_1}(p+q)n_{M_2}(p-q)(1+\zeta n_M(k))(1+\zeta n_{M_3}(2p-k)) \right. \\ & \left. - (1+\zeta n_{M_1}(p+q))(1+\zeta n_{M_2}(p-q))n_M(k)n_{M_3}(2p-k) \right], \end{aligned} \quad (16)$$

where

$$\begin{aligned} F(M, M_1, M_2, M_3) = & \sum_{n=0}^M \sum_{n_1=0}^{M_1} \sum_{n_2=0}^{M_2} \sum_{n_3=0}^{M_3} \\ & \mathcal{C}(n, n_1, n_2, n_3) \mathcal{C}(M-n, M_1-n_1, M_2-n_2, M_3-n_3) \end{aligned} \quad (17)$$

Fig. 3 shows how the total band populations $N_M = (M+1) \int n_M(k)dk$ evolve with time, starting from the initial state $n_M(k) = (0.4/(M+1))(\tanh[20(0.1+k)] + \tanh[20(0.1-k)])$ for $M = 0, 1, 2$, and 0 otherwise. Note that k is expressed in units of $1/d$. In Fig. 4 we plot the evolution of the total momentum state occupations $N(k) = \sum_M (M+1)n_M(k)$ for the same initial conditions. We see that N_M reaches a thermal profile within ~ 30 collision times, whereas it takes ~ 200 collision times for $N(k)$ to thermalize. We have tested different initial distributions, and find that these equilibration times do not vary appreciably as long as more than one energy level is populated.

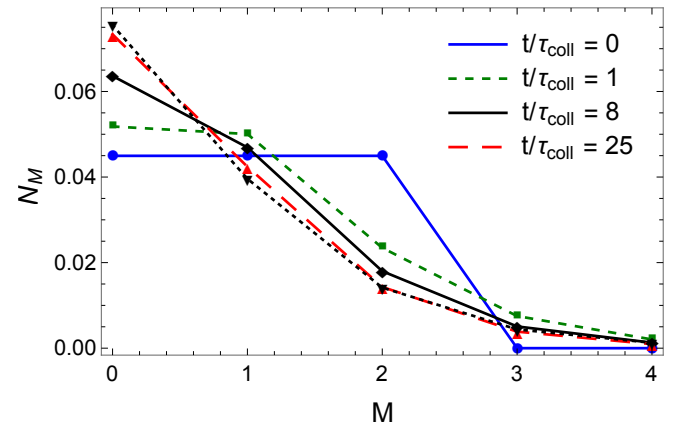


FIG. 3. Time evolution of the total populations in different energy levels, N_M . The dotted black line shows the thermal distribution with the same total particle number and energy.

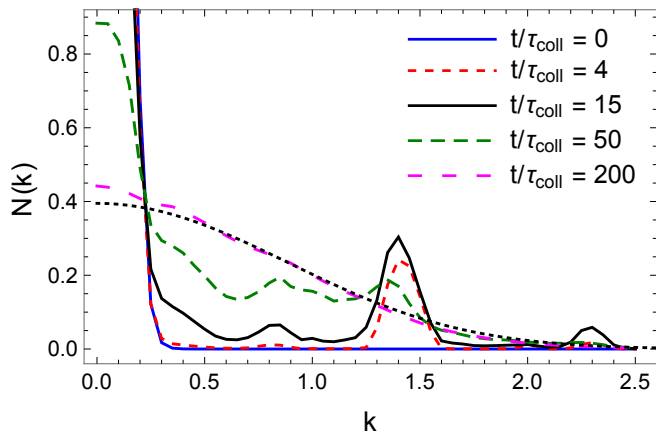


FIG. 4. Time evolution of the momentum distribution $N(k)$. The dotted black line shows the thermal distribution with the same total particle number and energy.

More interestingly, we see from Fig. 4 that the nature of thermalization for $N(k)$ is qualitatively different from all the other cases we have discussed. In contrast to the gradual diffusion-like behavior we observed in Fig. 1, we find that at short times, $N(k)$ develops a secondary peak at $k \approx \sqrt{2}$. As time passes, this peak grows gradually, and new tertiary peaks appear at $k \approx 0.87$ and $k \approx 2.3$. With time, these peaks spread out in either directions and overlap with one another, leading to a thermal profile at long times. We can explain the appearance of these peaks by examining the redistribution of momenta in two-body elastic collisions. Let us consider a collision between two particles with initial states $(M_1, p+q)$, $(M_2, p-q)$, and final states (M, k) , $(M_3, 2p-k)$. The collision conserves total energy. Therefore, in units of $\hbar\omega$, we can write $k^2 + (2p-k)^2 = 2(p^2 + q^2) + 2\Delta M$, where $\Delta M = M + M_3 - M_1 - M_2$. ΔM can only assume values $0, \pm 2, \pm 4, \dots$. This is because F in Eqs. (16)-(17) vanishes unless $M + M_1 - M_2 - M_3$ is even. Physically, this occurs because the even and odd numbered levels of the harmonic oscillator have opposite parity. Initially, all the particles have momenta close to zero. Thus $p, q \approx 0$. The dominant process which populate high momentum states comes from $\Delta M = 2$, for which we get $k = \sqrt{2}$. This gives rise to the secondary peak at short times in Fig. 4. Once a particle has scattered into the $k = \sqrt{2}$ state, it can then collide with a $k = 0$ particle. The dominant redistribution process for such a collision again comes from $\Delta M = 2$, which gives the new set of momenta at $k \approx 0.87$ and 2.3 . Thus we find tertiary peaks around these values in Fig. 4. These peaks are small because the population at $k = \sqrt{2}$ is much smaller than at $k = 0$. The distinct momentum values generated in binary collisions soon proliferate, which cause the different peaks to overlap, and eventually form a thermal profile. Future experiments can probe the multi-peaked momentum distribution which can be resolved for $\sim 50\tau_{\text{coll}}$.

Conclusions.—In conclusion, we have modeled ther-

malization in quasi-1D quantum gas experiments using kinetic rate equations. In the experiment, particles are captured in an array of elongated tubes oriented along the z direction by turning on a deep lattice in the x - y plane. We have considered two different scenarios. In one, the lattice is turned on adiabatically, as in [5, 6], and in the other, it is turned on suddenly. In the first case, the particles are confined to the lowest band. Here thermalization occurs because the different Bloch states within the band have slightly different energies, measured by the tunneling amplitude \tilde{J} . In a binary collision, the colliding particles can change their z -momenta by small amounts by scattering to different Bloch states. This allows the particles to reach all momentum states after sufficiently many collisions, which leads to thermal equilibrium. In the limit of small \tilde{J} we find that the momentum occupations evolve according to a diffusion-like equation (Eqs. (10)-(12)), and gradually approaches a thermal profile (Fig. 1). The thermalization rate is given by $m\omega^2 a_s^2 \tilde{J}^2 (a - b \ln \tilde{J}) + \mathcal{O}(\tilde{J}^4 \ln \tilde{J})$ where m is the particle mass, ω is the transverse confinement frequency, a_s is the scattering length, and the coefficients a and b grow with the particle density. From our numerics we estimate that the equilibration times in the experiments [5] and [6] are respectively much smaller and much larger than the measurement timescales. This justifies why the experimental data agree with thermodynamic calculations in the former, and the lack of thermalization observed in the latter.

If instead the lattice potential is turned on suddenly, the particles will be excited to several higher bands. We consider the case of a deep lattice, and model the subsequent dynamics by replacing the bands by discrete energy levels of a 2D harmonic confinement. We find three different timescales in the dynamics. The degenerate states within a level attain equal population within a few collision times (τ_{coll}). The different energy levels thermalize with one another in $\sim 30\tau_{\text{coll}}$, and the z -momentum states take the longest to equilibrate ($\sim 200\tau_{\text{coll}}$). The evolution of the momentum distribution $N(k)$ in this case is qualitatively different. Instead of gradually spreading out like a diffusion, $N(k)$ develops isolated peaks which grow, and eventually merge with one another to form a thermal profile (Fig. 4). This behavior originates from the discreteness of the energy levels which only allows the z -momenta of particles to change in jumps in binary collisions. Future experiments can probe this non-equilibrium multi-peaked momentum distribution.

In the present paper we treat the particle-particle interactions as a perturbation which causes transitions among the single-particle states. Thus our formalism is valid when the interactions do not fundamentally alter the system's behavior. It would be useful to extend our work to the strongly interacting domain in future work.

Appendix A: Simplifying the rate equation

When the particles are confined to the lowest band, the full rate equation governing the occupations of the momentum states is given in Eq. (7). With $n^\sigma(\vec{k}) = n(k)$ we can write

$$\begin{aligned} \frac{dn(k)}{d\tau} &= \int_{-\pi}^{\pi} \frac{d\tilde{k}_x}{2\pi} \int_{-\pi}^{\pi} \frac{d\tilde{k}_y}{2\pi} \frac{dn(\tilde{k})}{d\tau} \\ &= \frac{1}{\tilde{J}} \int_{-\infty}^{\infty} dp \int_{-\infty}^{\infty} dq \times \\ &\left[n(k+p)n(k+q)(1+\zeta n(k))(1+\zeta n(k+p+q)) - \right. \\ &\left. (1+\zeta n(k+p))(1+\zeta n(k+q))n(k)n(k+p+q) \right] \\ &\int_{-\pi}^{\pi} \frac{d\tilde{k}_x}{2\pi} \int_{-\pi}^{\pi} \frac{d\tilde{k}_{x1}}{2\pi} \int_{-\pi}^{\pi} \frac{d\tilde{k}_{x2}}{2\pi} \int_{-\pi}^{\pi} \frac{d\tilde{k}_y}{2\pi} \int_{-\pi}^{\pi} \frac{d\tilde{k}_{y1}}{2\pi} \int_{-\pi}^{\pi} \frac{d\tilde{k}_{y2}}{2\pi} \\ &\delta\left(\frac{pq}{\tilde{J}} + \cos \tilde{k}_{x1} + \cos \tilde{k}_{x2} - \cos \tilde{k}_x - \cos(\tilde{k}_{x1} + \tilde{k}_{x2} - \tilde{k}_x) \right. \\ &\left. + \cos \tilde{k}_{y1} + \cos \tilde{k}_{y2} - \cos \tilde{k}_x - \cos(\tilde{k}_{y1} + \tilde{k}_{y2} - \tilde{k}_y) \right), \end{aligned} \quad (\text{A1})$$

where $\tau = 2m\omega^2 a_s^2 / (\pi\hbar)$. Using the integral representation of the Dirac delta function we can write the six-dimensional integration over the quasimomenta as

$$f\left(\frac{pq}{\tilde{J}}\right) = \frac{1}{2\pi} \int_{-\infty}^{\infty} e^{i\frac{pq}{\tilde{J}}u} (g(u))^2, \quad (\text{A2})$$

where

$$\begin{aligned} g(u) &= \int_{-\pi}^{\pi} \frac{dx}{2\pi} \int_{-\pi}^{\pi} \frac{dy}{2\pi} \int_{-\pi}^{\pi} \frac{dz}{2\pi} e^{iu(\cos x + \cos y - \cos z - \cos(x+y-z))} \\ &= \int_{-\pi}^{\pi} \frac{dx}{2\pi} \int_{-\pi}^{\pi} \frac{dy}{2\pi} \int_{-\pi}^{\pi} \frac{dz}{2\pi} \int_{-\infty}^{\infty} \frac{d\alpha}{2\pi} \int_{-\infty}^{\infty} d\beta \\ &\quad \times e^{i[\beta(x+y-z-\alpha) + u(\cos x + \cos y - \cos z - \cos \alpha)]} \\ &= \int_{-\infty}^{\infty} d\beta \sum_{n=-\infty}^{\infty} e^{2\pi i n \beta} \left| \int_{-\infty}^{\infty} \frac{dx}{2\pi} e^{i(u \cos x + \beta x)} \right|^4 \\ &= \int_{-\infty}^{\infty} d\beta \sum_{n=-\infty}^{\infty} \delta(\beta - n) \left| \int_{-\infty}^{\infty} \frac{dx}{2\pi} e^{i(u \cos x + \beta x)} \right|^4 \\ &= \sum_{n=-\infty}^{\infty} \left| \int_{-\infty}^{\infty} \frac{dx}{2\pi} e^{i(u \cos x + nx)} \right|^4 \\ &= \sum_{n=-\infty}^{\infty} (J_n(u))^4 = {}_2F_3\left(\frac{1}{2}, \frac{1}{2}; 1, 1, 1; -4u^2\right). \end{aligned} \quad (\text{A3})$$

Here J_n denotes the Bessel function, and ${}_2F_3$ denotes the Hypergeometric function. Substituting Eq. (A3) into Eq. (A1) and rescaling the momenta p and q to $\tilde{J}^{\frac{1}{2}}p$ and $\tilde{J}^{\frac{1}{2}}q$ yield the expressions in Eq. (8) and (9).

Appendix B: Asymptotic expansion of the rate equation

Fourier transforming both sides of Eq. (8) we get

$$\dot{\tilde{n}}(x) = (\dot{\tilde{n}}(x))_{\text{cl}} + (\dot{\tilde{n}}(x))_{\text{qu}}, \quad (\text{B1})$$

where $\dot{\tilde{n}}(x) \equiv d\tilde{n}(x)/d\tau$, and

$$\begin{aligned} (\dot{\tilde{n}}(x))_{\text{cl}} &= \frac{2}{\pi} \int_{-\infty}^{\infty} d\xi \int_{-\infty}^{\infty} dy f(\xi) \tilde{n}(y) \tilde{n}(x-y) \\ &\quad \times \text{Re} \left[K_0\left(2\sqrt{\xi \tilde{J} y(x-y)}\right) - K_0\left(2\sqrt{\xi \tilde{J} y^2}\right) \right], \quad (\text{B2}) \\ (\dot{\tilde{n}}(x))_{\text{qu}} &= \frac{\zeta}{\pi^2} \int_{-\infty}^{\infty} d\xi f(\xi) \int_{-\infty}^{\infty} dx_1 \int_{-\infty}^{\infty} dx_2 \\ &\tilde{n}(x_1) \tilde{n}(x_2) \tilde{n}(x-x_1-x_2) \text{Re} \left[K_0\left(2\sqrt{\xi \tilde{J} x_1 x_2}\right) + \right. \\ &\left. K_0\left(2\sqrt{\xi \tilde{J}(x-x_1)(x-x_2)}\right) - 2K_0\left(2\sqrt{\xi \tilde{J} x_1(x-x_2)}\right) \right]. \end{aligned} \quad (\text{B3})$$

Here K_0 denotes the modified Bessel function, and Re denotes the real part. Since we have assumed that the momentum distribution $n(k)$ has a width large compared to $\tilde{J}^{\frac{1}{2}}$, its Fourier transform $\tilde{n}(x)$ will have a width smaller than $1/\tilde{J}^{\frac{1}{2}}$. In addition, we note that \tilde{J} is small, and the function $f(\xi)$ limits ξ to lie within ± 8 . Therefore, all arguments of K_0 in the above equation are small. Thus we can expand Eq. (B3) in powers of \tilde{J} using

$$\begin{aligned} K_0(\sqrt{z}) + \text{Re} K_0(i\sqrt{z}) \\ = -2\gamma - \ln(z/4) + (z^2/64)(3 - 2\gamma - \ln(z/4)) + \mathcal{O}(z^4) \end{aligned} \quad (\text{B4})$$

for small positive z , where γ is the Euler's constant. We then perform an inverse Fourier transform to obtain the asymptotic expansion in Eqs. (10)-(12), where the functionals $\mathcal{F}_i[n(k)]$, $i = 1, 2, 3, 4$ are given by

$$\mathcal{F}_1[n(k)] = (n''(k))^2 - n(k)n^{(4)}(k), \quad (\text{B5})$$

$$\begin{aligned} \mathcal{F}_2[n(k)] &= n(k) \int_0^{\infty} dp \ln p (n^{(5)}(k+p) - n^{(5)}(k-p)) \\ &\quad - n''(k) \int_0^{\infty} dp \ln p (n^{(3)}(k+p) - n^{(3)}(k-p)), \end{aligned} \quad (\text{B6})$$

$$\begin{aligned} \mathcal{F}_3[n(k)] &= \\ &\quad - \frac{n(k)}{3} [6(n''(k))^2 + 16n'(k)n^{(3)}(k) + 5n(k)n^{(4)}(k)], \end{aligned} \quad (\text{B7})$$

$$\begin{aligned} \mathcal{F}_4[n(k)] &= 2(\ln 2 - \gamma) \\ &\quad \times \partial_k^2 \left((n(k))^2 n^{(3)}(k) - 2(n'(k))^3 - 2n(k)n'(k)n''(k) \right) \\ &\quad + \partial_k^2 \left((n(k))^2 \int_0^{\infty} dp \ln p (n^{(4)}(k+p) - n^{(4)}(k-p)) \right. \\ &\quad \left. - n'(k) \partial_k^3 \int_0^{\infty} dp \ln p ((n(k+p))^2 - (n(k-p))^2) \right), \end{aligned} \quad (\text{B8})$$

where ∂_k denotes the derivative with respect to k , and $n^{(i)}(k) \equiv \partial_k^i n(k)$.

-
- [1] I. Bloch, J. Dalibard, and W. Zwerger, *Rev. Mod. Phys.* **80**, 885 (2008).
- [2] B. Paredes, A. Widera, V. Murg, O. Mandel, S. Fölling, I. Cirac, G. V. Shlyapnikov, T. W. Hänsch, and I. Bloch, *Nature* **429**, 277 (2004).
- [3] H. Moritz, T. Stöferle, M. Köhl, and T. Esslinger, *Phys. Rev. Lett.* **91**, 250402 (2003).
- [4] H. Moritz, T. Stöferle, K. Günter, M. Köhl, and T. Esslinger, *Phys. Rev. Lett.* **94**, 210401 (2005).
- [5] Y. Liao, A. S. C. Rittner, T. Paprotta, W. Li, G. B. Partridge, R. G. Hulet, S. K. Baur, and E. J. Mueller, *Nature* **467**, 567 (2010).
- [6] T. Kinoshita, T. Wenger, and D. S. Weiss, *Nature* **440**, 900 (2006).
- [7] M. A. Cazalilla, A. F. Ho, and T. Giamarchi, *New J. Phys.* **8**, 158 (2006).
- [8] G. Orso, *Phys. Rev. Lett.* **98**, 070402 (2007).
- [9] X.-J. Liu, H. Hu, and P. D. Drummond, *Phys. Rev. A* **76**, 043605.
- [10] M. Casula, D. M. Ceperley, and E. J. Mueller, *Phys. Rev. A* **78**, 033607 (2008).
- [11] E. Zhao and W. V. Liu, *Phys. Rev. A* **78**, 063605 (2008).
- [12] K. Yang, *Phys. Rev. B* **63**, 140511(R) (2001).
- [13] P. Kakashvili and C. J. Bolech, *Phys. Rev. A* **79**, 041603(R) (2009).
- [14] X.-W. Guan, M. T. Batchelor, and C. Lee, *Rev. Mod. Phys.* **85**, 1633 (2013).
- [15] M. Rigol, *Phys. Rev. Lett.* **103**, 100403 (2009).
- [16] M. Rigol, *Phys. Rev. A* **80**, 053607 (2009).
- [17] M. Rigol, V. Dunjko, and M. Olshanii, *Nature* **452**, 854 (2008).
- [18] A. Polkovnikov, K. Sengupta, A. Silva, and M. Vengalattore, *Rev. Mod. Phys.* **83**, 863 (2011).
- [19] I. E. Mazets and J. Schmiedmayer, *New J. Phys.* **12**, 055023 (2010).
- [20] C. Chin, R. Grimm, P. Julienne, and E. Tiesinga, *Rev. Mod. Phys.* **82**, 1225 (2010).
- [21] D. Guéry-Odelin, *Phys. Rev. A* **66**, 033613 (2002).
- [22] D. Jaksch, C. Bruder, J. I. Cirac, C. W. Gardiner, and P. Zoller, *Phys. Rev. Lett.* **81**, 3108 (1998).